NANO LETTERS

Letter

pubs.acs.org/NanoLett

Size-Dependent Photoionization in Single CdSe/ZnS Nanocrystals

Kevin T. Early† and David J. Nesbitt*

JILA, National Institute of Standards and Technology and University of Colorado, Department of Chemistry and Biochemistry, University of Colorado Boulder, Boulder, Colorado 80309, United States

Supporting Information

ABSTRACT: Fluorescence intermittency in single semiconductor nanocrystals has been shown to follow power law statistics over many decades in time and in probability. Recently, several studies have shown that, while "off" dwell times are insensitive to almost all experimental parameters, "on" dwell times exhibit a pump-power dependent exponential truncation at long times, suggestive of enhanced biexciton photoionization probabilities at high excitation powers. Here we report the dependence of this on-time truncation on nanocrystal radius. We observe a decrease in the per-pulse photoionization probability from $1.8(2) \times 10^{-4}$ to $2.0(7) \times 10^{-6}$ as the CdSe core radius increases from 1.3 to 3.5 nm, with a radius scaling for the probability for charge ejection arising from biexciton formation $P_{\text{ionize}}(r) \propto 1/r^{3.5(5)}$. Effective mass calculations of the exciton wave functions show that the product of fractional electron and hole probabilities in the trap-rich ZnS shell scale similarly with nanocrystal radius. Possible charge ejection mechanisms from such a surface-localized state are discussed.

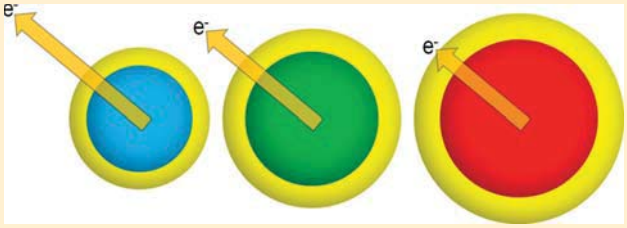

KEYWORDS: *Quantum dots, blinking, photoionization, Auger, carrier relaxation*

Fluorescence intermittency, or blinking, in single semiconductor nanocrystals (NCs) has been studied extensively since the first reports by Brus and co-workers.[1] Despite being problematic for applications that benefit from consistently high quantum yield emission, such as biological tracking,[2] quantum dot lasers,[3−5] and nanocrystal-based display technologies,[6] blinking has been a valuable tool for investigating intrinsic single NC photoluminescence dynamics. Correlations between blinking events and discrete spectral jumps[7] implicate ionization as a likely contributor to intermittency, as further evidenced by charging of single NCs after extended periods of illumination[8] and photodarkening of quantum dot glasses.[9] Dwell time analysis of both bright and dark states has revealed an enormous range of time scales for intermittency,[10] the probabilities of which were shown to be power law distributed with an exponent $m \approx -1.5$. Such a nonexponential distribution indicates a distributed trapping state picture, in which charge ejection and return rates vary over many orders of magnitude.[11,12] Studies of the effects of dielectric environment on single NC blinking have revealed a sensitivity of the power law exponent on the medium in which the NCs are deposited,[13] indicating the relative importance of external trap sites to the blinking process.

In addition to pure power law behavior, deviations from power-law distributed dwell times for fluorescent ("on") states have been observed in single NCs. In particular, dwell times for on-states τ_{on} follow a power law at short times but at longer times begin to truncate exponentially. The form of this truncated power law distribution is described by $P(\tau_{on}) = A\,\tau_{on}^{-m}\exp(-k_{on}\tau_{on})$, where k_{on} is the exponential rate constant for the truncation at long times and m is the power law exponent. This truncation represents a significant addition to the pure power law kinetic picture, which contains no intrinsic time scale for charge ejection and reneutralization. However, several conflicting reports about the underlying mechanism responsible for this truncation exist. Crouch et al.[14] have reported truncation times that are insensitive to excitation energy or NC size, whereas Shimizu et al.[15] observe a truncation that is sensitive to NC size, capping conditions, and temperature. Stefani et al.[16] observe truncation times that are dependent on the substrate on which individual NCs are deposited. Knappenberger et al.[17] find purely power-law distributed on times when exciting directly into the $1S_e-1S_h$ band edge state, with truncation occurring at higher-energy excitation, suggesting a thermal contribution to the process dictating this exponential behavior, and Cordones et al. have found truncation behaviors in both on- and off-times that depend on both wavelength and excitation power.[18] Peterson and Nesbitt[19] have reported a quadratic increase in the characteristic truncation time with increasing excitation intensity, which was attributed to the Poisson-distributed generation of multiexcitons even under modest excitation conditions.

In this paper, we report on the size dependence of photoionization from single CdSe/ZnS NCs under relatively low excitation powers, as determined by analyzing the truncation behavior of the on-time probability distribution with increasing excitation power. The power dependence of the

Received: July 15, 2013
Revised: September 4, 2013
Published: September 10, 2013

truncation time is examined as a function of excitation power and NC core size, and the per-pulse photoionization efficiencies are calculated assuming Poisson statistics for multiexciton generation. The photoionization efficiencies are shown to scale with NC core radius as $1/r^{3.5(5)}$. To aid in the analysis of these results, electron and hole wave functions are calculated in the effective mass approximation. It is found that the product of fractional electron and hole probabilities within the NC shell scale similarly with core radius, suggesting an enhanced charge ejection probability when two charge carriers are localized near the NC surface. The implications for charge ejection mechanisms are discussed.

Experiment. Single quantum dot detection is performed on a raster scanning inverted confocal fluorescence microscope, as shown schematically in Figure 1. In brief, laser excitation from a

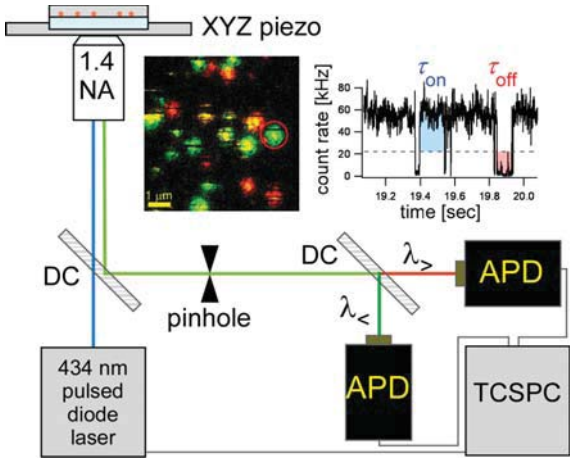

Figure 1. Schematic experimental setup. Fluorescence from single NCs is collected and sent into long- and short-wavelength detection channels ($\lambda_>$ and $\lambda_<$). A representative raster scan and single molecule trajectory with individual on (τ_{on}, blue) and off (τ_{on}, red) intervals are shown. DC, dichroic filter; NA, numerical aperture; APD, avalanche photodiode; TCSPC, time-correlated single photon counting module.

434 nm pulsed diode laser is circularly polarized with a $\lambda/4$ plate, expanded using a telescoping lens pair, and coupled into a high numerical aperture (NA = 1.4) oil immersion objective, resulting in a nearly diffraction limited laser spot (d = 230 nm). Fluorescence from individual NCs is passed through a confocal pinhole and imaged onto two avalanche photodiodes (APDs), with a dichroic beamsplitter centered at the bulk NC emission peak sorting emitted photons by emission wavelength. All photons are tagged with an arrival time relative to the laser pulse, a global time, and a channel stamp, providing dynamical information relative to the laser pulse as well as the wall clock. Experiments are carried out on a size series of CdSe/ZnS NCs (NN-Laboratories, with core radii ranging from 1.3 to 3.5 nm). Single NCs are diluted to 500−1000 pM in a solution of 0.3% (w/v) PMMA in toluene and spin-cast onto ozone-cleaned glass coverslips at 1500 rpm, yielding surface coverage densities of ∼0.2 NCs/μm^2.

Results. Figure 2 (left panel) shows a series of partial fluorescence trajectories for a single NC (QD580) under increasing laser excitation power at λ = 434 nm (P = 38, 55, and 90 nW from top to bottom). Trajectories are generated by binning macroscopic arrival times into 1 ms time bins to permit determination of an on/off count rate threshold, which is

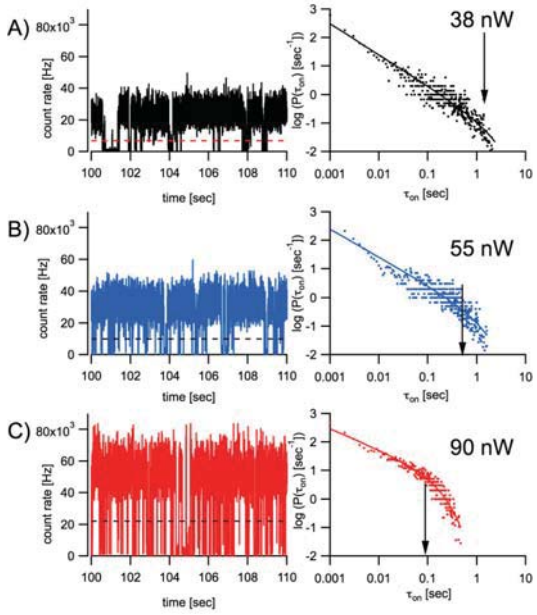

Figure 2. Partial fluorescence trajectories (left) and corresponding "on" dwell time probability densities P(τ_{on}) (right) for a single QD580 NC at excitation power (A) P = 38 nW, (B) 55 nW, and (C) 90 nW. On−off thresholds are shown as dashed lines overlaid on trajectories. The arrows on the probability density plots indicate the exponential rolloff time constant t_{on}.

generally set to the minimum between average "on" and "off" intensity levels in a count rate histogram. Qualitatively, the number of on/off switching events in a given time interval increases with increasing laser intensity. The differences in fluorescence dynamics are most clearly observed in the corresponding on-time probability densities (right panel), where again excitation powers range from P = 38 nW (top) to P = 90 nW (bottom). At low pump powers, probability densities are power law distributed over all time scales, with the form $P(\tau_{on}) = A\tau_{on}^{-m}$. With increasing laser intensity, the on-time probability densities roll off at large τ_{on}. As seen in the P = 90 nW probability density plot, the onset of the truncation occurs near 100 ms, after which the relative number of long on-dwell times quickly decrease. Probability densities are fit by a truncated power law of the form $P(\tau_{on}) = A\tau_{on}^{-m}\exp(-k_{on}\tau_{on})$, where $1/k_{on}$ is the time constant of the exponential roll off. Fluorescence trajectories are recorded for 1000 s to ensure adequate sampling of low-probability long "on" dwell time events. As shown recently,[20] artifacts associated with under-sampling can skew determination of the truncation rate constant, and attempts to mitigate these effects have been devised.[21] In these studies, raw probability densities are fit using weighted nonlinear least-squares to the truncated power law form above to extract the amplitude A, power law exponent m, and k_{on}. Some 50−100 NCs at each excitation power are fit using this method, and the average truncation rate constant $\langle k_{on}\rangle$ at each power is determined.

The dependence of $\langle k_{on}\rangle$ on NC absorption rate for two sizes of NCs (r = 1.3 nm (green) and 1.5 nm (blue)) is shown in Figure 3A, where $\langle k_{on}\rangle$ refers to the average exponential rate constant at a given absorption rate for a number of single NCs, and the error bars represent the standard deviation of the mean. We plot $\langle k_{on}\rangle$ as a function of absorption rate ($\Gamma_{abs} = I\sigma/h\nu$) instead of excitation intensity to account for changes in the NC

dx.doi.org/10.1021/nl402607a | Nano Lett. 2013, 13, 4844−4849

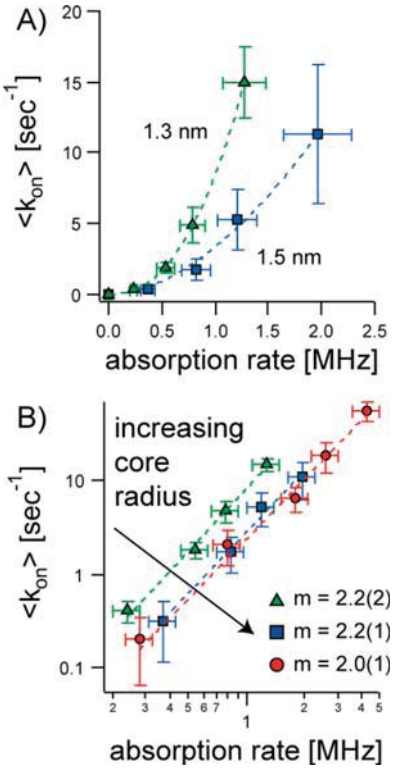

Figure 3. (A) $\langle k_{on} \rangle$ versus NC absorption rate for NCs with radii indicated, as denoted by the symbols. Absorption rates are reported to account for differences in NC absorption cross section. (B) Data for NCs of radii 1.3, 1.5, and 2.1 nm plotted on a log−log scale, showing approximately quadratic dependence of $\langle k_{on} \rangle$ on the NC absorption rate. The slopes from the linear fits are given.

absorption cross section with increasing core radius. Error bars in the absorption rate arise from the width of the $1S_e-1S_{3/2}$ absorption band edge obtained in bulk absorption measurements. A clear nonlinear increase in $\langle k_{on} \rangle$ is observed with increasing excitation power for both NC species shown. This nonlinearity is clearly depicted in Figure 3B, where the plots are shown on a log−log scale. Linear fits to the data on the log−log plot yield slopes of 2.2(2), 2.2(1), and 2.0(1) for NCs of radii 1.3, 1.5, and 2.1 nm, respectively, and indicate a clear quadratic dependence of the truncation rate constant on excitation power. This dependence has been demonstrated previously[19] for both continuous wave and pulsed illumination and multiple excitation wavelengths.

Following the analysis first described by Peterson and Nesbitt,[19] per-pulse photoionization probabilities are determined by examining the pump power dependence of the truncation rate constant. In brief, the average exciton number $\langle N \rangle = I\sigma/h\nu$ generated in a single NC at the low excitation intensities used in these studies (10−100 nW) is small (on the order of 10^{-3}), with a Poisson-distributed probability $P_{\langle N \rangle}(n) = \exp^{-\langle N \rangle}\langle N \rangle^n/n!$ of forming higher exciton numbers n per pulse (i.e., $O(10^{-6})$ for $n > 1$). However, with a laser repetition rate of 5 MHz, the time scale for forming multiple excitons becomes shorter than typical experimental on-dwell times (1 ms and longer). In the limit $\langle N_{exc} \rangle \ll 1$, we can Taylor expand the above equation and invert to obtain the average number of pulses required to generate an n-exciton state, and multiplication by the interpulse duration ΔT_{pulse} yields the time scale for multiexciton formation τ_{MX},

$$\tau_{MX} \approx \frac{2\Delta T_{pulse}}{\langle N_{exc} \rangle^2}$$

This analysis correctly predicts the quadratic dependence of the multiexciton-induced truncation rate constant of the on-dwell time distribution with increasing excitation intensity. Rearranging to give the number of per-pulse ionization events and scaling by a factor corresponding to the photoionization efficiency arising from biexciton generation P_{ionize},

$$\Delta T_{pulse} k_{MX} \approx P_{ionize} \frac{\langle N_{exc} \rangle^2}{2}$$

Equating k_{MX} to our experimentally observed truncation rate constant k_{on}, plots of $\Delta T_{pulse} \times k_{on}$ versus $(1/2)\langle N_{exc} \rangle^2$ yield lines with slopes P_{ionize}. Figure 4 shows photoionization plots

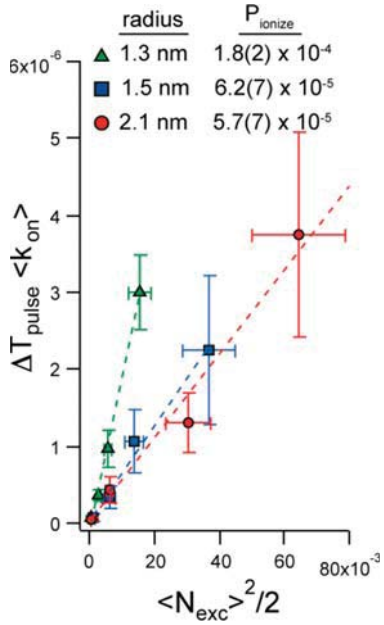

Figure 4. Plots of $\Delta T_{pulse} \times k_{on}$ versus$\langle N_{exc} \rangle^2/2$ for the size series of NCs indicated, along with photoionization probabilities obtained from linear fits of the data (dashed lines).

for three different NC core radii with linear fits. For the three NC sizes shown, the photoionization efficiency per pulse decreases with increasing core radius, from $1.8(2) \times 10^{-4}$ to $5.7(7) \times 10^{-5}$ going from $r = 1.3$ to 2.1 nm.

The dependence of the photoionization efficiency on NC core radius is shown in Figure 5. A decrease in P_{ionize} from $1.8(2) \times 10^{-4}$ to $2(7) \times 10^{-6}$ is observed for NC core radii ranging from 1.3 to 3.5 nm. In the inset, a linear fit of the data on a log−log plot reveals a decrease in the photoionization probability that scales as $P_{ionize}(r) \propto r^{-3.5(5)}$, where the error is obtained from the least-squares fit. These results are consistent with reports by Klimov and co-workers,[22,23] who observe an increase in the Auger constant that scales with NC volume as determined from bulk transient absorption measurements.

Discussion. Having observed photoionization probabilities consistent with Auger volume scaling in these nanocrystals, we have calculated quantum-confined charge carrier wave functions to further elucidate the sign of the charge carrier being ejected. Recent electrochemical studies of single nanocrystals by Galland et al. have indicated that the ejected carrier is a

dx.doi.org/10.1021/nl402607a | Nano Lett. 2013, 13, 4844−4849

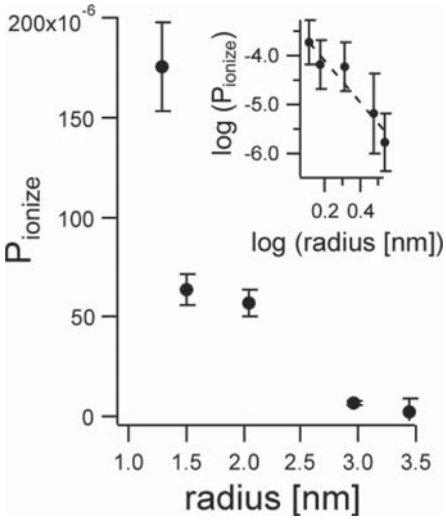

Figure 5. Photoionization probability P_{ionize} as a function of NC core radius, determined from the slopes of the plots in Figure 4. Probabilities span from 1.8(2) × 10^{-4} to 1.7(7) × 10^{-6}. Error bars represent the standard deviation from the fits. Inset: Same data on a log–log plot. The dashed line is a linear fit, yielding a slope m = −3.5(5).

hole.[24] Wavefunctions for CdSe/ZnS heterostructures were calculated within the effective mass approximation following the methods outlined by Haus et al.[25] and Schooss et al.[26] (see Supporting Information). Assuming spherical symmetry for electrons and holes and neglecting Coulomb terms (assuming strong confinement, where the confinement term dominates), the carrier wave function is separable according to $\Psi_{nlm}(r,\theta,\phi) = R_{nl}(r)Y_l^m(\theta,\phi)$, where n, l, and m label the principal and angular momentum quantum numbers.

The calculated radial electron (black) and hole (red) wave functions for the smallest NC studied here are shown in Figure 6. Due to their smaller effective masses, electrons are

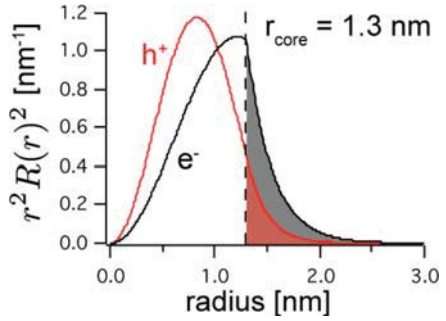

Figure 6. Calculated electron (black) and hole (red) radial wave functions for a NC of core radius 1.3 nm, marked with a dashed vertical line. The shaded regions to the right of the line represent the electron and hole probability density within the ZnS shell. See text for details of calculation.

delocalized further into the ZnS shell than holes. Because the highest density of trap states likely occurs near the CdSe/ZnS interfacial and in the ZnS interface owing to alloying dislocations, the quantity of interest is the fractional probability of a carrier in this region. The importance of the core–shell interfacial region on Auger recombination has been studied in great detail for alloyed CdSe/CdSeS/CdS heterocrystals, and alloying effects were shown to have significant impact on the volume scaling of Auger processes.[27] Similar analyses have been applied to CdSe/ZnS NCs with varying shell thicknesses to study recombination kinetics as a function of electron–hole spatial wave function overlap[28] and to CdSe/CdS particles to study the effects of exchange interactions on degeneracy breaking of the band-edge exciton state.[29] We define the fractional probability $f_{e(h)}$ for an electron (hole) to reside in the ZnS shell by

$$f_{e(h)}(a) \equiv \int_{r=a}^{\infty} r^2 R_{e(h)}{}^2(r)\, dr$$

where $R_{e(h)}{}^2$ is the normalized electron (hole) radial wave function. With decreasing probability density in the capping layer, this quantity decreases with increasing core radius for both electrons and holes. This fractional probability is represented in Figure 6 as the shaded region beyond $r = a$.

Here we consider a number of cases corresponding to the numbers of charge carriers in the trapping region. In Figure 7, we plot (A) f_e, (B) $f_e f_h$, and (C) $f_e f_h f_e$, corresponding to fractional probability (or product thereof) of a single electron, an electron–hole pair, and an electron–hole pair with an extra electron in the shell region, respectively, as a function of NC core radius. For an Auger photoionization event, one might expect the photoionization probability to scale like the three-carrier probability density in the trapping region. However, the three-carrier product $f_e f_h f_e$ scales with core radius as $r^{-5.7}$, inconsistent with our experimental observations of photoionization efficiency scaling. Instead, the product of the electron and hole fractional probabilities $f_e f_h$ scales as $1/r^{3.5}$, in good agreement with experimental data, and appears to dictate charge carrier ejection efficiency from the quantum dot core. In Figure 7D, the photoionization probability and the quantity $f_e f_h$ are plotted together and normalized to the values for the smallest NC studied, $P_{ionize,0}$ and $f_e f_{h,0}$, respectively. In this picture, the simultaneous localization of an electron and hole in the NC shell leads to ejection of an additional charge carrier with a small probability on a per-exciton formation basis. Due to the smaller effective mass of the electron, we hypothesize that the ejected carrier is negatively charged; however, these experiments do not lend direct evidence for this. Further photoionization studies in high electric fields are currently being undertaken to aid in the experimental determination of the sign of the ejected particle.

Such NC surface states have been shown to be important in interfacial electron transfer processes occurring in a polarizable small-molecule bath,[30] in the presence of nearby electron-acceptor molecules,[28] and in hybrid polymer–semiconductor nanoparticles.[31] As well, Frantsuzov and Marcus[32] have developed an electron transfer rate theory that is dependent on diffusion of the $1S_e$–$1P_e$ intraband electron energy level spacing, which should be highly sensitive to surface effects due to the spatial extent of the P-like electron wave function. In this report, the nature of the charge-trapped final states is not explicitly treated; instead, ejection occurring from a prepared initial state is assumed. Clearly, treatment of ionized final states in a Fermi's golden rule treatment, such as that by Rabani and Baer[33] for multiexciton formation, would provide a more complete picture.

In addition to the radius scaling of the photoionization efficiency, the relative magnitudes of P_{ionize} and $f_e f_h$ contain information on the competing charge carrier pathways available to surface-localized charge carriers. Analogous to quantum yield

dx.doi.org/10.1021/nl402607a | Nano Lett. 2013, 13, 4844–4849

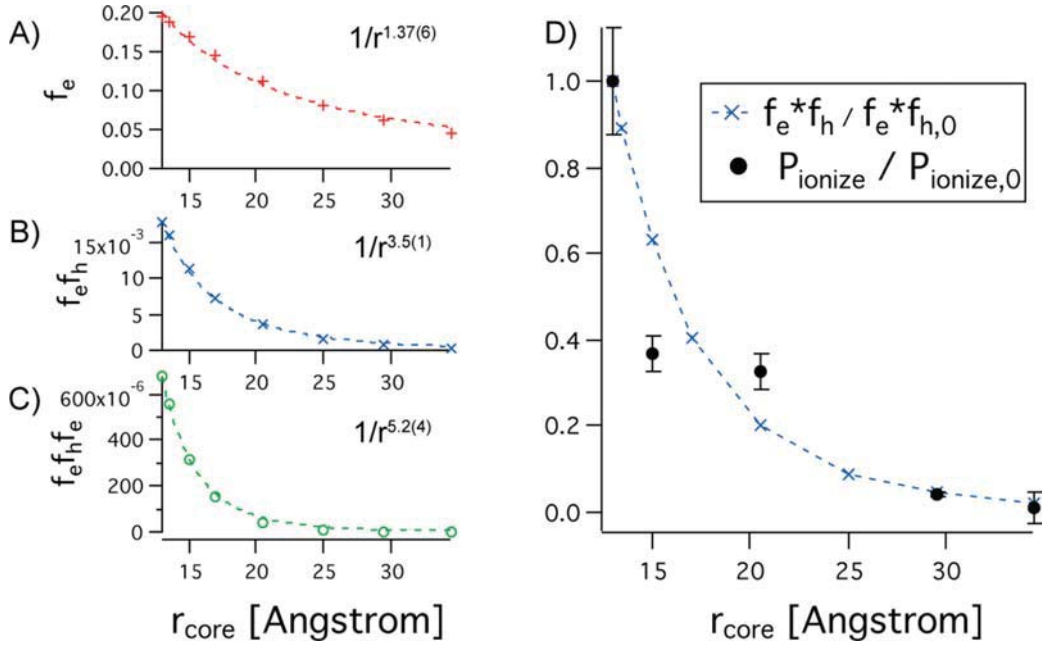

Figure 7. (A) Integrated fractional probability in the ZnS for a single electron, f_e, as a function of NC core radius. (B) The product of single electron and hole fractional shell probabilities $f_e f_h$ and (C) the electron−hole fractional probability product with an extra electron as a function NC core radius. The scaling of the fractional probabilities with core radius is indicated in each case. (D) Experimental P_{ionize} values (black circles) and calculated values of $f_e f_h$ (X's with dashed line) as a function of NC core radius, scaled to the values for the smallest-radius NC studied (P_{ionize},0 and $f_e f_{h,0}$, respectively).

definitions, the yield for photoionization can be determined at each NC size. If we equate the electron−hole fractional probability product $f_e f_h$ with the population of charge carriers in the trapping region, the photoionization yield can be defined as

$$P_{ionize} = f_e f_h \frac{k_{ionize}}{(k_{ionize} + k_{relax})}$$

where k_{ionize} and k_{relax} are the rates for ionization and relaxation from the two-particle surface state. The quantity $P_{ionize}/f_e f_h$ then represents the fraction of photoionization events occurring from the surface state. From the values of P_{ionize} measured for each NC radius, the average photoionization fraction $P_{ionize}/f_e f_h$ = 0.8(4)%, where the uncertainty gives the standard deviation from the measurements of P_{ionize}. While Auger relaxation appears to be the dominant pathway for escape from the surface-localized exciton state, roughly 1% of the exciton population in this state undergoes charge ejection and formation of the dark, nonfluorescent state of the NC. It should be noted here that the above analysis refers only to pulsed excitation, where the photoionization probabilities are on a per-pulse basis; continuous wave excitation leads to *per-fluorescence lifetime* photoionization probabilities, with lower average exciton numbers at a given excitation intensity than for pulsed excitation. While this analysis provides some insight into the mechanism underlying charge ejection, the calculated values are sensitive to the level of the model used to calculate the quantity $f_e f_h$.

We note that, while these results are consistent with those observed by Klimov and co-workers,[4] other experiments by Chepic, et al. have indicated a much stronger dependence of the photoionization rate on nanocrystal radius for CdS quantum dots embedded in glasses.[9] Whether this discrepancy in photoionization size scaling arises from the stronger quantum confinement in CdS than in CdSe (bulk band gaps 2.6 of eV and 1.7 eV) or from effects of the surrounding dielectric environment is unclear. However, in the current experiments, statistics are generated for single NCs by counting durations of sequential luminescent and charge-ejected states and requires that the nanocrystal avoid photodestruction for periods of tens of minutes. In comparison to the case of an ensemble of NCs embedded in glass, we may be selecting those NCs which are highly resistant to photobleaching and thus also resistant to anomalous volume scaling effects.

Conclusion. A systematic study of per-pulse photoionization probability with increasing nanocrystal core radius has shown a decrease of roughly 2 orders of magnitude in efficiency as the CdSe core radius increases from 1.3 to 3.5 nm. The photoionization probability has been found to scale as $1/r^{3.5(5)}$ over the NC sizes studied. To better understand this trend, effective mass wave functions were calculated for electrons and holes for a series of CdSe/ZnS NCs with increasing radius, where localization of charge carriers in the trap-rich ZnS shell region decreases as the core diameter increases. We find good agreement between experimentally observed photoionization efficiency scaling and the scaling of the product of fractional probabilities of a single electron and single hole in the ZnS shell, suggesting that localization of an exciton near the NC surface is necessary for ejection of a charge carrier through an Auger photoionization process. A comparison of steady-state population of these surface-localized states and experimental values of photoionization probabilities indicates that roughly 1% of surface localized states lead to ionization.

dx.doi.org/10.1021/nl402607a | *Nano Lett.* 2013, 13, 4844−4849

■ ASSOCIATED CONTENT

Supporting Information

Wavefunction calculations and supporting references. This material is available free of charge via the Internet at http://pubs.acs.org.

■ AUTHOR INFORMATION

Corresponding Author

*E-mail: djn@jila.colorado.edu.

Present Address

†3M, St. Paul, Minnesota 55144, United States.

Notes

The authors declare no competing financial interest.

■ ACKNOWLEDGMENTS

This work has been supported by the National Science Foundation (CHE1012685, PHYS1125844) and the National Institute for Standards and Technology. K.T.E. would also like to gratefully acknowledge financial support from the National Institute for Standards and Technology for a National Research Council Postdoctoral Fellowship.

■ REFERENCES

(1) Nirmal, M.; Dabbousi, B. O.; Bawendi, M. G.; Macklin, J. J.; Trautman, J. K.; Harris, T. D.; Brus, L. E. *Nature* **1996**, *383*, 802.

(2) Dahan, M.; Levi, S.; Luccardini, C.; Rostaing, P.; Riveau, B.; Triller, A. *Science* **2003**, *302*, 442.

(3) Klimov, V. I.; Ivanov, S. A.; Nanda, J.; Achermann, M.; Bezel, I.; McGuire, J. A.; Piryatinski, A. *Nature* **2007**, *447*, 441.

(4) Klimov, V. I.; Mikhailovsky, A. A.; Xu, S.; Malko, A.; Hollingsworth, J. A.; Leatherdale, C. A.; Eisler, H. J.; Bawendi, M. G. *Science* **2000**, *290*, 314.

(5) Malko, A. V.; Mikhailovsky, A. A.; Petruska, M. A.; Hollingsworth, J. A.; Htoon, H.; Bawendi, M. G.; Klimov, V. I. *Appl. Phys. Lett.* **2002**, *81*, 1303.

(6) Coe, S.; Woo, W. K.; Bawendi, M.; Bulovic, V. *Nature* **2002**, *420*, 800.

(7) Neuhauser, R. G.; Shimizu, K. T.; Woo, W. K.; Empedocles, S. A.; Bawendi, M. G. *Phys. Rev. Lett.* **2000**, *85*, 3301.

(8) Krauss, T. D.; Brus, L. E. *Phys. Rev. Lett.* **2000**, *84*, 1638.

(9) Chepic, D. I.; Efros, A. L.; Ekimov, A. I.; Vanov, M. G.; Kharchenko, V. A.; Kudriavtsev, I. A.; Yazeva, T. V. *J. Lumin.* **1990**, *47*, 113.

(10) Kuno, M.; Fromm, D. P.; Hamann, H. F.; Gallagher, A.; Nesbitt, D. J. *J. Chem. Phys.* **2001**, *115*, 1028.

(11) Kuno, M.; Fromm, D. P.; Hamann, H. F.; Gallagher, A.; Nesbitt, D. J. *J. Chem. Phys.* **2000**, *112*, 3117.

(12) Kuno, M.; Fromm, D. P.; Johnson, S. T.; Gallagher, A.; Nesbitt, D. J. *Phys. Rev. B* **2003**, 67.

(13) Cichos, F.; von Borczyskowski, C.; Orrit, M. *Curr. Opin. Colloid Interface* **2007**, *12*, 272.

(14) Crouch, C. H.; Mohr, R.; Emmons, T.; Wang, S. Y.; Drndic, M. *J. Phys. Chem. C* **2009**, *113*, 12059.

(15) Shimizu, K. T.; Neuhauser, R. G.; Leatherdale, C. A.; Empedocles, S. A.; Woo, W. K.; Bawendi, M. G. *Phys. Rev. B* **2001**, 63.

(16) Stefani, F. D.; Knoll, W.; Kreiter, M.; Zhong, X.; Han, M. Y. *Phys. Rev. B* **2005**, 72.

(17) Knappenberger, K. L.; Wong, D. B.; Romanyuk, Y. E.; Leone, S. R. *Nano Lett.* **2007**, *7*, 3869.

(18) Cordones, A. A.; Bixby, T. J.; Leone, S. R. *J. Phys. Chem. C* **2011**, *115*, 6341.

(19) Peterson, J. J.; Nesbitt, D. J. *Nano Lett.* **2009**, *9*, 338.

(20) Crouch, C. H.; Sauter, O.; Wu, X. H.; Purcell, R.; Querner, C.; Drndic, M.; Pelton, M. *Nano Lett.* **2010**, *10*, 1692.

(21) Frantsuzov, P. A.; Volkan-Kacso, S.; Janko, B. *Phys. Rev. Lett.* **2009**, 103.

(22) Klimov, V. I.; Mikhailovsky, A. A.; McBranch, D. W.; Leatherdale, C. A.; Bawendi, M. G. *Science* **2000**, *287*, 1011.

(23) Robel, I.; Gresback, R.; Kortshagen, U.; Schaller, R. D.; Klimov, V. I. *Phys. Rev. Lett.* **2009**, 102.

(24) Galland, C.; Ghosh, Y.; Steinbruck, A.; Hollingsworth, J. A.; Htoon, H.; Klimov, V. I. *Nat. Commun.* **2012**, *3*, 908.

(25) Haus, J. W.; Zhou, H. S.; Honma, I.; Komiyama, H. *Phys. Rev. B* **1993**, *47*, 1359.

(26) Schooss, D.; Mews, A.; Eychmuller, A.; Weller, H. *Phys. Rev. B* **1994**, *49*, 17072.

(27) Garcia-Santamaria, F.; Brovelli, S.; Viswanatha, R.; Hollingsworth, J. A.; Htoon, H.; Crooker, S. A.; Klimov, V. I. *Nano Lett.* **2011**, *11*, 687.

(28) Zhu, H. M.; Song, N. H.; Lian, T. Q. *J. Am. Chem. Soc.* **2010**, *132*, 15038.

(29) Brovelli, S.; Schaller, R. D.; Crooker, S. A.; Garcia-Santamaria, F.; Chen, Y.; Viswanatha, R.; Hollingsworth, J. A.; Htoon, H.; Klimov, V. I. *Nat. Commun.* **2011**, *2*, 280.

(30) Jones, M.; Lo, S. S.; Scholes, G. D. *Proc. Natl. Acad. Sci. U.S.A.* **2009**, *106*, 3011.

(31) Hammer, N. I.; Early, K. T.; Sill, K.; Odoi, M. Y.; Emrick, T.; Barnes, M. D. *J. Phys. Chem. B* **2006**, *110*, 14167.

(32) Frantsuzov, P. A.; Marcus, R. A. *Phys. Rev. B* **2005**, 72.

(33) Rabani, E.; Baer, R. *Nano Lett.* **2008**, *8*, 4488.